Highly Stretchable and Tough Hydrogels below Water Freezing Temperature

Xavier P. Morelle, Widusha R. Illeperuma, Kevin Tian, Ruobing Bai, Zhigang Suo, and Joost J. Vlassak*

Hydrogels consist of hydrophilic polymer networks dispersed in water. Many applications of hydrogels rely on their unique combination of solid-like mechanical behavior and water-like transport properties. If the temperature is lowered below 0 °C, however, hydrogels freeze and become rigid, brittle, and non-conductive. Here, a general class of hydrogels that do not freeze at temperatures far below 0 °C, while retaining high stretchability and fracture toughness, is demonstrated. These hydrogels are synthesized by adding a suitable amount of an ionic compound to the hydrogel. The present study focuses on tough polyacrylamide-alginate double network hydrogels equilibrated with aqueous solutions of calcium chloride. The resulting hydrogels can be cooled to temperatures as low as −57 °C without freezing. In this temperature range, the hydrogels can still be stretched more than four times their initial length and have a fracture toughness of 5000 J m^{-2}. It is anticipated that this new class of hydrogels will prove useful in developing new applications operating under a broad range of environmental and atmospheric conditions.

Hydrogels are crosslinked networks of hydrophilic polymer chains dispersed in water. The polymer network gives the hydrogels solid-like mechanical properties, while the aqueous phase enables fast diffusion, endowing the hydrogels with liquid-like transport properties. Along with these attributes, many hydrogels are also biocompatible, making them traditional materials of choice for tissue engineering and drug delivery systems.[1] Recent works have considerably enlarged the range of applications of hydrogels by improving their stretchability and toughness up to the level of natural rubbers.[2,3] The combination of exceptional toughness, large stretchability, optical transparency, and high ionic conductivity has led to the development of many new applications in the field of hydrogels, including

stretchable and transparent ionic conductors,[4] fire-resistant fabrics,[5] stretchable electroluminescent devices,[6] ionic skin and touch panels,[7,8] and soft robotic actuators.[9] However, in all these applications, the hydrogels lose their desirable properties once the temperature decreases below the freezing point of water, severely limiting their use in this temperature range. Recently, organic liquids such as propylene or ethylene glycol have been used to synthesize hybrid organo-hydrogels with an improved working temperature range.[10] There are concerns, however, about the environmental impact and health hazard as a result of the toxicity of these liquids.[11] Here, we present another class of hydrogels that retain their stretchability, toughness, and conductivity at temperatures far below 0 °C.[12] These nonfreezing hydrogels rely on the colligative property of ionic compounds such as calcium chloride ($CaCl_2$) to depress the freezing point of the aqueous phase.[12–15] Freezing point depression is of course a well-known phenomenon with many applications in cold environments. For example, $CaCl_2$ is widely used to prevent roads from icing over.[15] The same phenomenon also allows a number of organisms, including many insects and some wood frogs, to survive extremely cold weather conditions by preventing the formation of ice crystals in their cells.[16] Electrical conductivity of salt-containing polyacrylamide hydrogels have been measured at temperatures below 0 °C, but their mechanical behavior has not been studied.[17] In the present study, we synthesized a series of polyacrylamide-alginate double network hydrogels, and soaked them in three different aqueous $CaCl_2$ solutions (see the Experimental Section for preparation details and Figure S1, Supporting Information). Depending on the concentration of the $CaCl_2$ soaking solution, these hydrogels froze over a range of temperatures from 0 °C down to approximately −57 °C. We measured the mechanical response of these $CaCl_2$-containing double network hydrogels over a broad range of temperatures, from ambient down to −70 °C, and distinguished three types of behavior depending on the state of the gel: i) regular *hydrogel* behavior when the aqueous phase is in the liquid state, ii) *slurry gel* behavior when the aqueous phase is in a partially frozen state that consists of a mixture of ice crystals and salt solution, and iii) *frozen gel* behavior when the aqueous phase is fully frozen. We also characterized the temperature dependence of the fracture toughness of these hydrogels. We discovered

Dr. X. P. Morelle, Dr. W. R. Illeperuma, K. Tian, Dr. R. Bai,
Prof. Z. Suo, Prof. J. J. Vlassak
John A. Paulson School of Engineering and Applied Sciences
Harvard University
Cambridge, MA 02138, USA
E-mail: vlassak@seas.harvard.edu
Dr. X. P. Morelle, Dr. R. Bai, Prof. Z. Suo
Kavli Institute for Bionano Science and Technology
Cambridge, MA 02138, USA
Dr. X. P. Morelle
Soft Matter Science and Engineering Laboratory
ESPCI ParisTech, Paris 75005, France

The ORCID identification number(s) for the author(s) of this article
can be found under https://doi.org/10.1002/adma.201801541.
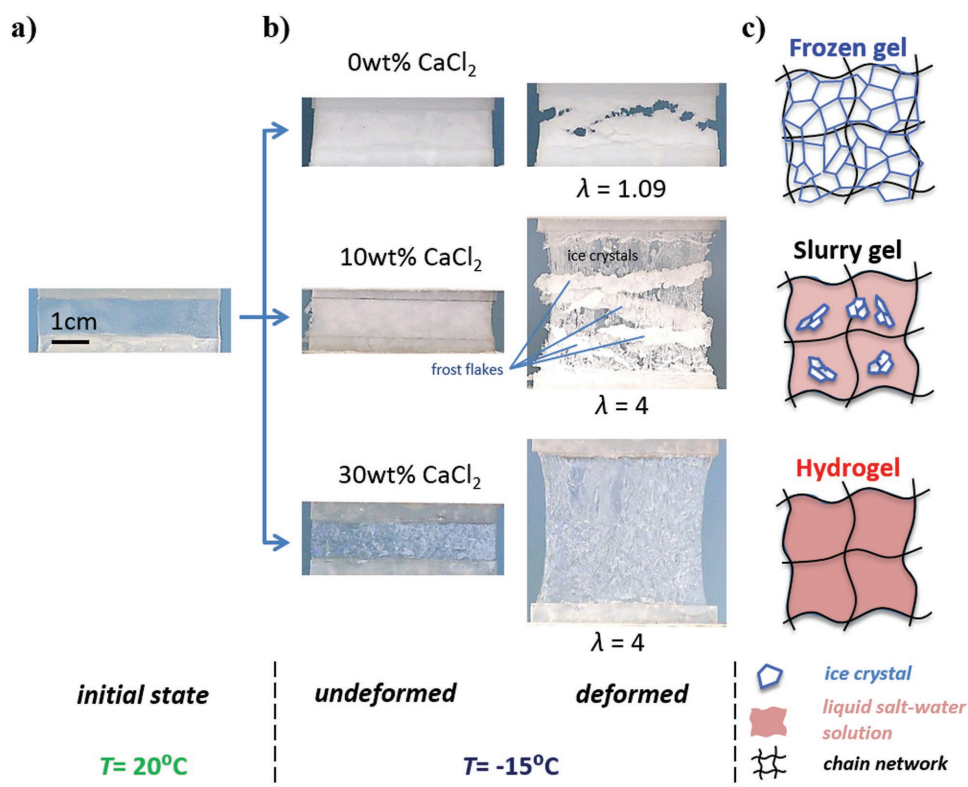
Figure 1. Hydrogel behavior in subzero environment illustrated for three different CaCl$_2$-containing gels: a) the initial state at room temperature, b) the undeformed and deformed state at −15 °C, and c) the corresponding molecular pictures. This illustrates the three physical states for a hydrogel below the freezing point of water: at −15 °C, the 0 wt% CaCl$_2$ gel is in the *frozen* state forming an opaque aggregate of ice crystals and polymer chains, the 10 wt% CaCl$_2$ gel is in the *slurry* state with a mixture of ice crystals and salt solution in a polymer network, and the 30 wt% CaCl$_2$ is in the regular *hydrogel* state with an aqueous phase in the liquid state. The frozen gel and slurry gel form a frost layer on their surfaces after cooling.

that a high fracture toughness (≈5000 J m^{-2}) can be obtained at temperatures as low as −50 °C (see Table S1, Supporting Information). In particular, slurry gels were found to have the highest toughness in subzero temperature conditions. By focusing on the gradual evolution of the fracture process in the slurry gels, we identified crack pinning and deflection, as well as distributed initiation of micro-damage, as additional toughening mechanisms. Finally, we confirmed that CaCl$_2$-containing hydrogels retain good ionic conductivity at low temperatures, and explored potential applications of these non-freezing hydrogels by demonstrating a simple touch sensing ionic panel that works at subzero temperatures.

Figure 1 illustrates the three distinct types of behavior observed for hydrogels with different CaCl$_2$ concentrations at the same subzero temperature. Despite similar behavior at room temperature, the three hydrogels behave very differently when they are cooled to −15 °C and deformed in tension (similar observations in compression are shown in Figure S2, Supporting Information). While the gel soaked in 30 wt% CaCl$_2$ behaves like a regular hydrogel with good stretchability and transparency at −15 °C, gels soaked in 0 and 10 wt% solutions behave differently. For the sake of brevity, we will refer to these different gel compositions in the rest of this manuscript by the concentration of their soaking solution, even if the actual ionic content in the gel may be slightly different. At −15 °C, the hydrogel with 0 wt% CaCl$_2$ is frozen solid, forming an opaque

aggregate of ice crystals and polymer chains. The frozen gel is stiff and brittle, and fractures at a relatively small strain (≈9%). At the same temperature, the hydrogel with 10 wt% CaCl$_2$ is a slurry gel: a gel consisting of a mixture of ice crystals and salt solution embedded in a polymer network. While the gel has lost most of its optical transparency, it remains as stretchable as the 30 wt% gel. The slurry gel behavior occurs over a wide range of temperatures. This observation is consistent with the binary phase diagram of CaCl$_2$ and water (**Figure 2**a), and leads to the experimental phase diagram of the polyacrylamide-alginate double network gel soaked in aqueous CaCl$_2$ solutions shown in Figure 2b. The slurry gel state corresponds to the two-phase region in the CaCl$_2$–water phase diagram, both areas are shaded in gray in the respective phase diagrams. As a hydrogel is progressively cooled through the two-phase region, the increasing opacity of the gel reflects the increasing volume fraction of ice crystals.

To construct the phase diagram in Figure 2b, we first collected all the experimental observations from the mechanical testing under different temperatures performed on hydrogels soaked in 0, 10, and 30 wt% CaCl$_2$ solutions, and identified the state of each gel based upon its mechanical response and optical transparency. These observations provided a discrete sampling of the phase diagram, depicted by the symbols in Figure 2b. In a second step, we characterized each gel composition and its various components using dynamic
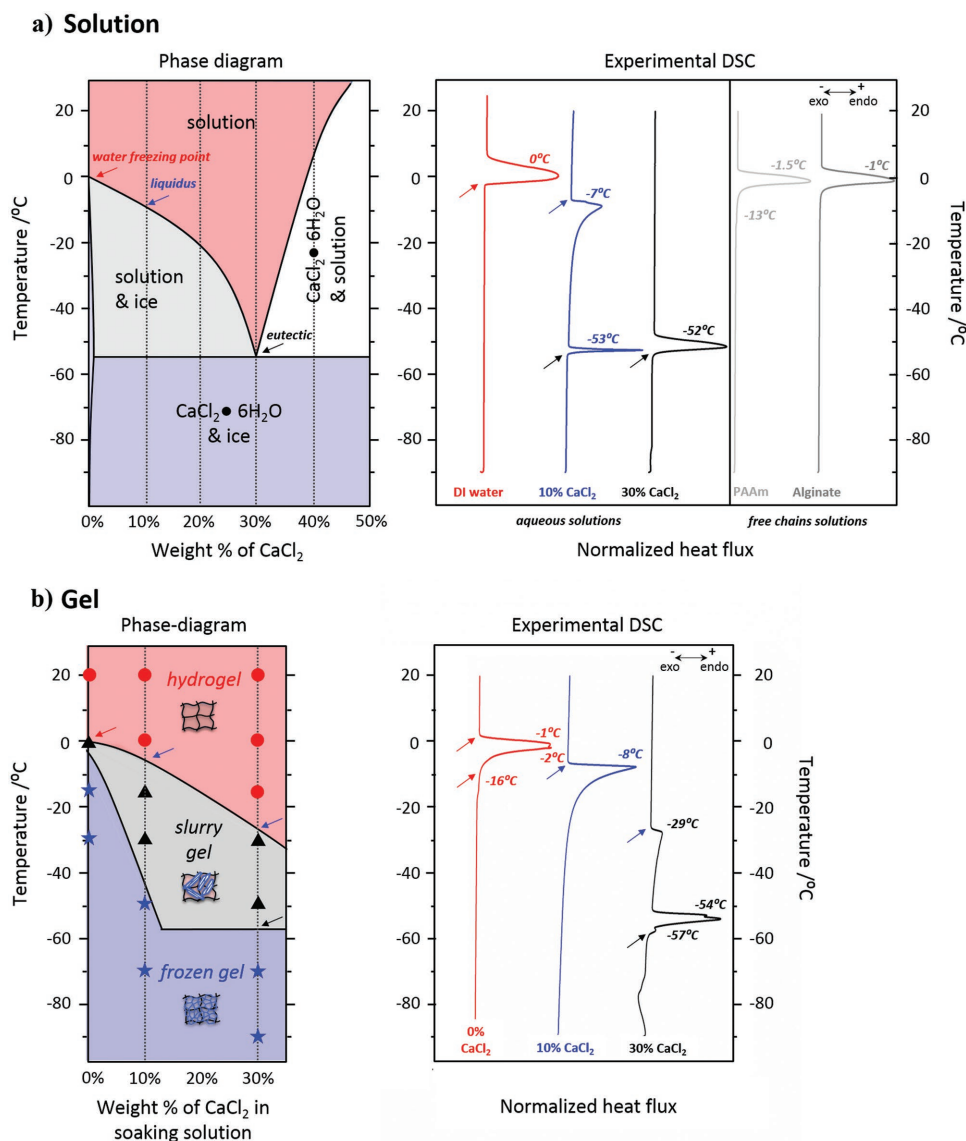
Figure 2. Phase diagram and experimental DSC of the aqueous $CaCl_2$ solution and the $CaCl_2$-containing gel. a) Aqueous $CaCl_2$ solution case: the theoretical phase diagram (left) is compared to the experimental DSC results (right). b) $CaCl_2$-containing gel case: the experimentally built phase diagram (left) is compared to the experimental DSC results for the three gel compositions (right). The small arrows highlight the correspondence between the phase boundaries in the phase diagram and the fusion enthalpy peaks in the experimental DSC runs.

scanning calorimetry (DSC) from −90 °C to room temperature to obtain a more accurate measurement of the boundaries of the various phase regions. We also performed DSC analyses on aqueous $CaCl_2$ solutions to identify the phase boundaries for the aqueous system, which were found to be consistent with the reported phase diagram[13] with only minor experimental deviations. Aqueous solutions of polyacrylamide and alginate were independently thermally characterized (Figure 2a, right) to assess the effect of the polymer chains on the freezing point of the solutions. Comparison of Figure 2a,b demonstrates that the DSC curve for the 0 wt% $CaCl_2$ gel can be regarded as the superposition of the curves for its constituents, with a double peak, a small shoulder, and a small shift of the liquidus to lower temperature. These peaks in the DSC curve indicate that the hydrogel behaves

like a ternary system rather than a simple binary. The calorimetry data in Figure 2b shows that the slurry region of the hydrogel is shifted to significantly higher $CaCl_2$ concentrations compared to the two-phase region of the aqueous $CaCl_2$ solution. Indeed, it is clear from the two distinct and separate peaks of the DSC curve that the 30 wt% $CaCl_2$ gel has not yet reached the eutectic composition. We hypothesize that this shift is the result of interactions of $CaCl_2$ with the alginate and polyacrylamide polymer chains in the gel and an indication that the equilibrium concentration of $CaCl_2$ inside the gel is lower than in the aqueous solution. Indeed, by weighing the fully dried residue of the different gel compositions, we estimated the actual concentration of $CaCl_2$ inside the 10 and 30 wt% $CaCl_2$ gel batches respectively as 5–7 and 20–23 wt% of $CaCl_2$.
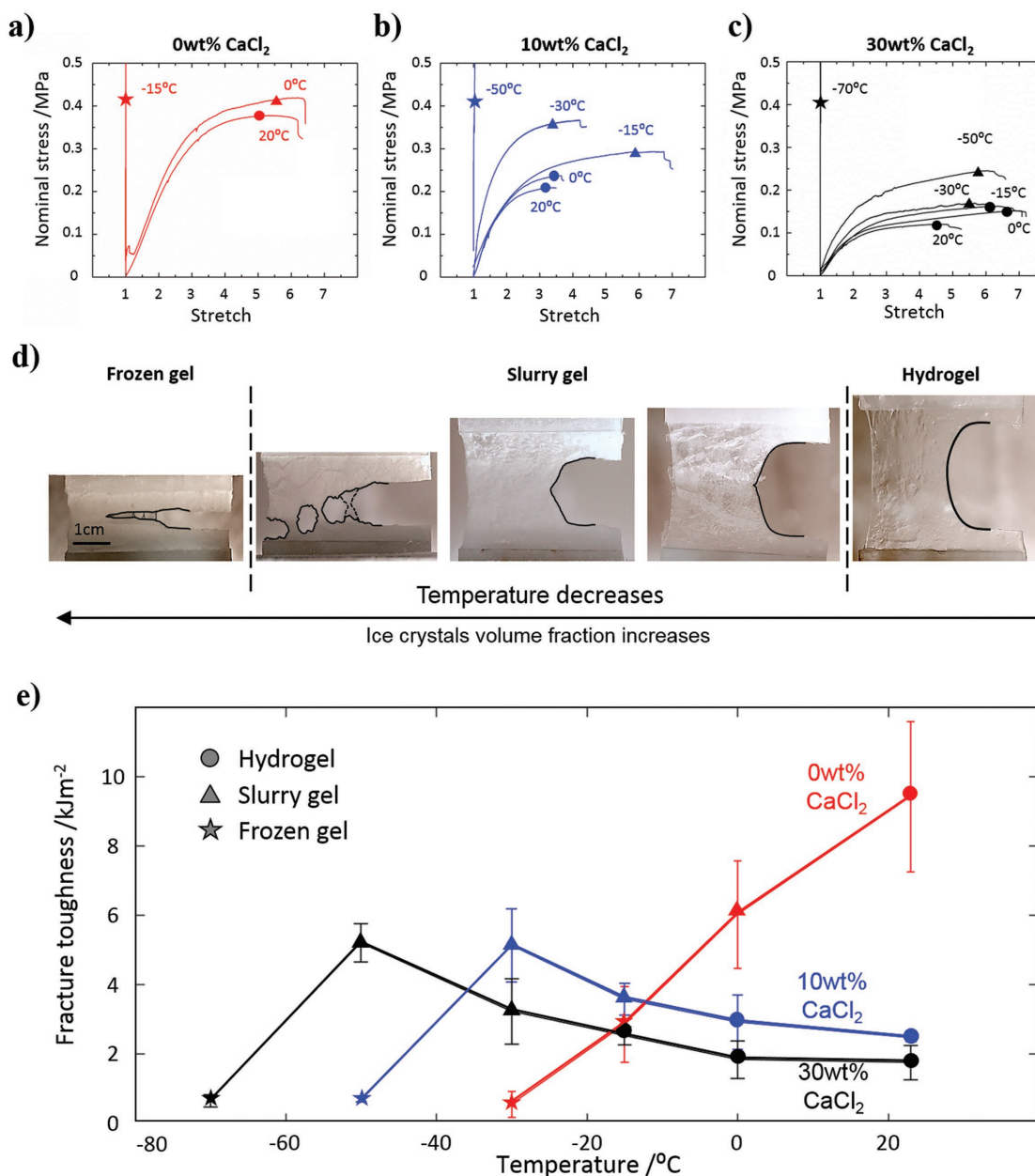
Figure 3. Mechanical characterization and fracture patterns of gels with different $CaCl_2$ content as function of temperature. The stress–stretch curves are measured at different temperatures for the three gels: a) 0 wt% $CaCl_2$, b) 10 wt% $CaCl_2$, and c) 30 wt% $CaCl_2$. d) The evolution of crack propagation profile in different $CaCl_2$-containing gels as the temperature decreases, and thus as the volume fraction of ice increases. Gel type and associated testing conditions from left to right are: i) 30 wt% at −70 °C, ii) 30 wt% at −70 °C (undercooled), iii) 10 wt% at −50 °C (undercooled), iv) 0 wt% at 0 °C, and v) 30 wt% at −15 °C. e) The fracture toughness of the three gels is characterized as a function of temperature. For each testing condition, symbols (circle, triangle, and star) indicate the corresponding physical state of the gel (hydrogel, slurry, and frozen gel, respectively).

Figure 3a–c shows the evolution of the stress–stretch curves with decreasing temperature for the 0, 10, and 30 wt% $CaCl_2$ gels, respectively (for complete experimental data, see Figure S3, Supporting Information). At room temperature, the 0 wt% $CaCl_2$ gel has the highest strength and stretchability. When the temperature is reduced to −15 °C, however, this gel becomes stiff and brittle. The 10 and 30 wt% $CaCl_2$ gels, on the other hand, retain their stretchability at temperatures down to at least −30 and −50 °C, respectively. For all gels, both the elastic modulus and the strength gradually increase as the temperature decreases. This stiffening effect can be explained by the gradual increase of the volume fraction of ice crystals in the slurry gel (Figure 3d). The ice crystals stiffen the gel, while still allowing large deformation to occur through shear yielding between them, similar to the toughening of polymer nanocomposites.[18] Interestingly, the presence of ice crystals tends to improve the stretchability before the gels become brittle (see evolution of fracture stretch in Table S2,

1801541 (4 of 8)

**ADVANCED
SCIENCE NEWS**

www.advancedsciencenews.com

**ADVANCED
MATERIALS**

www.advmat.de

Supporting Information). A careful inspection of post-mortem specimens showed a large number of micro-sized cavities dispersed throughout the specimens (Figure S4, Supporting Information). These micro-cavities may nucleate due to the triaxial state of stress that builds up around stiff ice crystals. A similar mechanism of cavitation and fracture has been reported in adhesively bonded elastic and viscoelastic layers.[19,20] From the study of adhesively bonded materials, cavitation first appears when the hydrostatic stress is approximately ten times larger than the shear modulus of the elastic layer.[20] The cavities grow and eventually coalesce, leading to catastrophic cohesive failure of the adhesive layer.[19] Growth of these cavities provides an additional energy dissipation mechanism that may explain the increased stretchability observed in the slurry state. This mechanism leads to the apparent "ductile" failure mode mechanism with macroscopic void growth and coalescence observed experimentally in specimens with large volume fractions of ice in the slurry state (see Figure 3d and Movie S5, Supporting Information). Further investigation showed that the nucleation of these micro-cavities is also facilitated by the application of repeated cooling cycles to very low temperature. Indeed, repeated formation of ice crystals eventually leads to a permanent weakening of the gel network, creating local defects that facilitate the nucleation of cavities upon deformation.

To characterize the fracture toughness of the gels as a function of temperature, we measured the stress–stretch curves of notched specimens and determined the critical stretch at which fast fracture takes place (Table S2, Supporting Information). We calculated the corresponding energy release rate by integrating the area under the nominal stress–stretch curve of a pure shear specimen without a precrack (from Figure 3a–c) up to the critical stretch of the notched specimens, following the method devised by Rivlin and Thomas.[3,21] The results show the temperature dependence of the fracture toughness for each gel (Figure 3e and Table S1, Supporting Information). As expected, the fracture toughness of the 0 wt% $CaCl_2$ gel reduces dramatically as the temperature is lowered below 0 °C. By contrast, the fracture toughness of the 10 and 30 wt% gels increases as the gels enter the slurry state. The fracture toughness of these gels eventually drops as the gels are fully frozen. For all gels, the slurry state exhibits a relatively high toughness, ranging from 3000 to 6000 J m^{-2}. In practical applications, the amount of salt added to a hydrogel can be adjusted to fulfill the requirements in terms of modulus, stretchability, and fracture toughness depending on the targeted temperature range.

In order to better understand the toughening mechanism associated with the slurry gels, we compare the crack propagation and failure scenarios in the three subzero states of the hydrogel (**Figure 4**). A regular hydrogel fails through
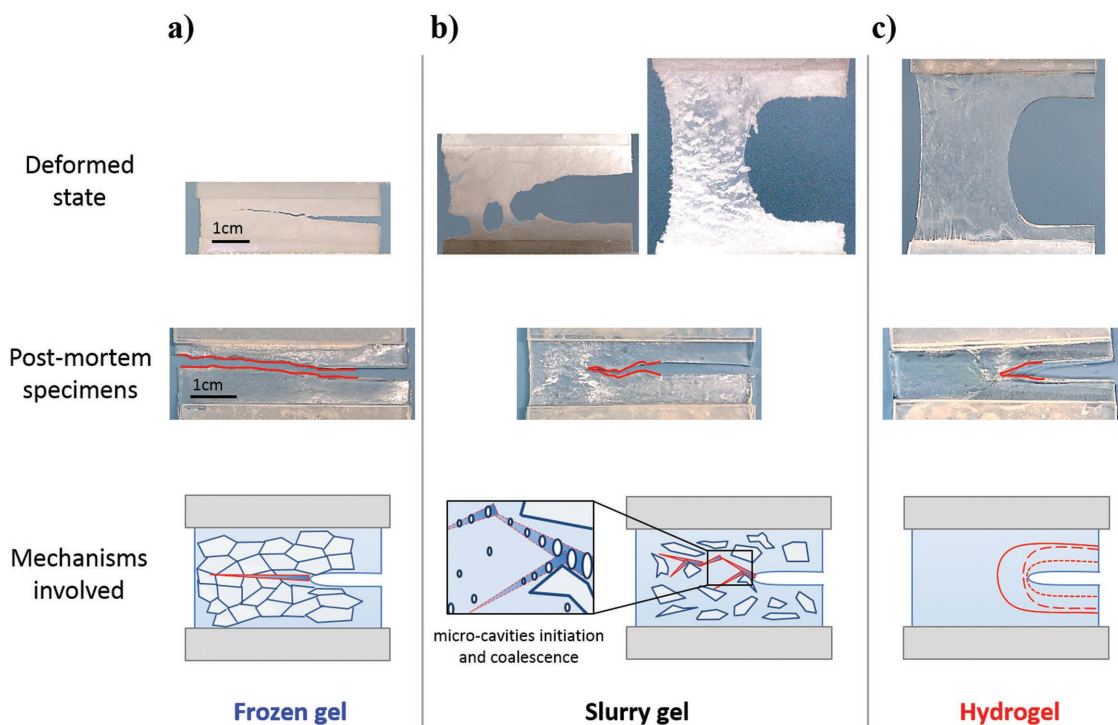
Figure 4. Different failure scenarios and the associated fracture mechanisms in the three states of a gel. a) For a frozen gel, brittle fracture occurs by fast propagation of a sharp crack following the straightest and weakest path between ice crystals. b) For a slurry gel, the fracture varies with the volume fraction of ice crystals, but typically shows a stick-slip propagation following a zig-zag path. A relatively large not fully blunted crack opening is observed (the middle and top right picture). Crack pining, crack deflection, and micro-cavitation have been identified as associated toughening mechanisms, sometimes leading to the coalescence of multiple macro-cracks in some samples (top left). c) For a regular tough hydrogel, a large blunted crack is observed during the crack propagation. The gels shown here to illustrate the fracture scenario of each of sub-water-freezing state of gels have been tested with the following conditions, from left to right: (a) 0 wt% $CaCl_2$ at −50 °C, (b-left) 30 wt% $CaCl_2$ at −70 °C (undercooled), (b-right and crack path) 10 wt% $CaCl_2$ at −30 °C, and (c) 0 wt% at 20 °C.

**ADVANCED
SCIENCE NEWS**
www.advancedsciencenews.com

**ADVANCED
MATERIALS**
www.advmat.de

the propagation of a large blunted crack (Figure 4c and Movie S2, Supporting Information). Slurry gels and frozen gels, however, exhibit significantly different failure mechanisms. In the frozen gel, a sharp crack propagates rapidly through the specimen once it is loaded, following the straightest and weakest path between ice crystals, resulting in a relatively low fracture toughness (Figure 4a and Movie S3, Supporting Information). The fracture behavior of slurry gels varies depending on the amount of ice crystals in the gel, but is typically characterized by crack pinning and deflection as the crack path encounters stiff ice crystals. Such features, observed in all slurry gels, lead to a discontinuous crack propagation, and sometimes a less blunted crack tip compared to the regular hydrogel state (Figure 4b, right, and Movie S4, Supporting Information). The final fracture path in a slurry gel tends to zigzag and creates rough crack surfaces. The amplitude of that zigzag and the degree of roughness of the crack surface varies depending on the ice volume fraction (i.e., the higher the volume fraction, the larger the zigzag). More specifically, in some slurry gels with a large volume fraction of ice, multiple macro-cracks grow upon loading, and eventually coalesce (Figure 4b, left, and Movie S5, Supporting Information). These macro-cracks are assumed to initiate at the dispersed micro-cavities observed ahead of the crack tip (Figure S4, Supporting Information) as mentioned earlier.

During the experiments, we observed significant undercooling of the slurry gels below the eutectic temperature, which can have a significant impact on the stability of subzero mechanical behavior of hydrogels. As shown in Figure S5 (Supporting Information) (and Movie S5, Supporting Information), a 30 wt% $CaCl_2$ gel can stay in an undercooled slurry state, and exhibit high stretchability and fracture toughness at temperatures as low as −70 °C if it is not cooled down long enough to reach thermodynamic equilibrium. The undercooled gels are thermodynamically unstable, and consequently have stress–stretch curves that vary inconsistently with the storage time at −70 °C (see Figure S5c, Supporting Information). To avoid this undercooling effect, all the testing specimens in this study were first cooled to −90 °C for 45 min before heating them to the target testing temperature. To conclude, the slurry state of $CaCl_2$-containing hydrogels at subzero temperatures can indeed provide unforeseen mechanical property improvements, but caution must be taken to ensure that the material is not in a thermodynamically unstable state due to a kinetic delay of the crystallization process.
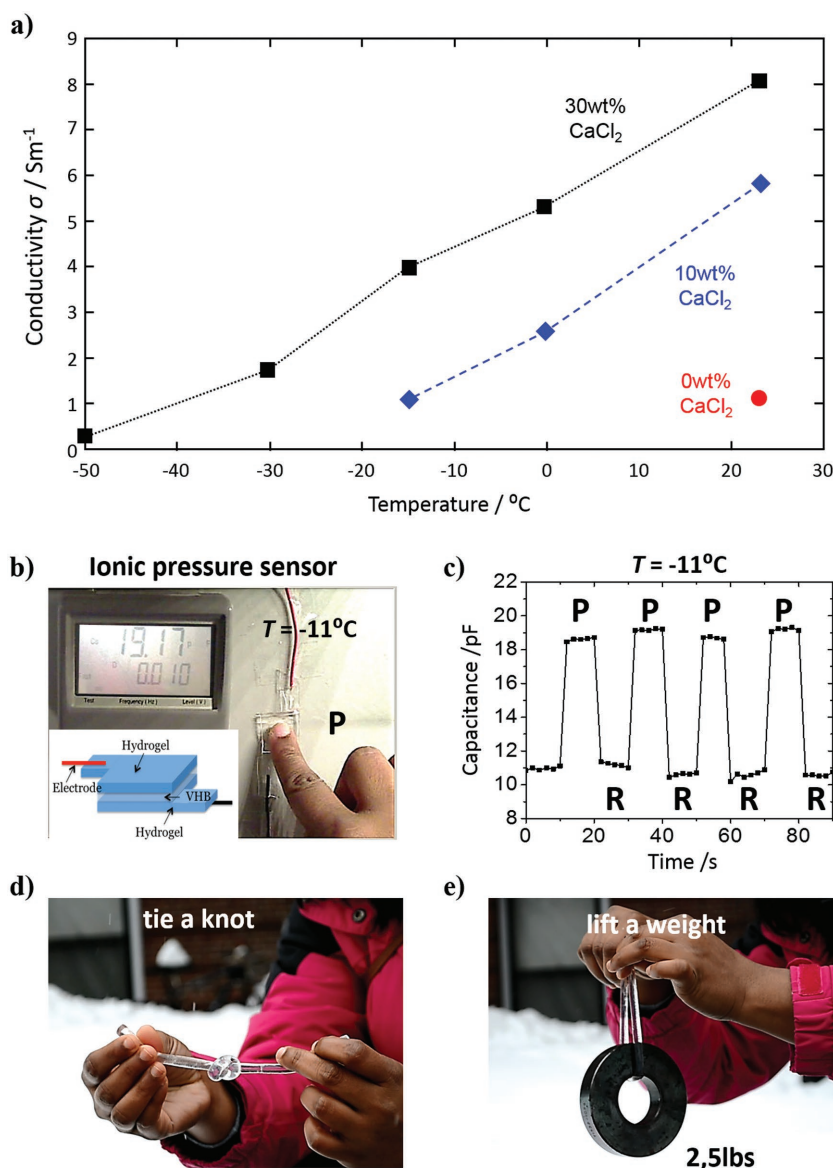
Figure 5. Applications of the stretchable, tough, and antifreezing hydrogel at low temperature. a) The conductivity as a function of temperature for the 0, 10, and 30 wt% $CaCl_2$ gels. b) A stretchable ionic touch sensor is fabricated by sandwiching a layer of dielectric elastomer (3M VHB) between two layers of 30 wt% $CaCl_2$ gels. c) The capacitance changes at −11 °C by a finger press and release. "P" denotes finger press and "R" denotes release. d,e) demonstrate the good stretchability and strength of a 30 wt% $CaCl_2$ gel in outdoor snowing conditions (associated video can be found in Movie S1, Supporting Information). The weight used is 2.5 lbs (1.13 kg).

The $CaCl_2$-containing gels maintain their ionic conductivity at temperatures well below the freezing point of water (**Figure 5**a). This ability, together with their high stretchability and toughness at low temperatures, opens up a range of applications in low-temperature environments. Here, we demonstrated a simple ionic touch sensor that takes advantage of both attributes. The touch sensor consists of a dielectric elastomer layer sandwiched between two hydrogel layers (Figure 5b). The hydrogel layers consist of 30 wt% $CaCl_2$ hydrogels, while the elastomer is VHB 4905 (3M, Maplewood MN). The architecture of the touch sensor is based on a sensor described previously

**ADVANCED
SCIENCE NEWS**

www.advancedsciencenews.com

**ADVANCED
MATERIALS**

www.advmat.de

by Sun et al.[7] Figure 5c illustrates the response of the sensor when operated at a temperature of −11 °C. The capacitance of the sensor changes reversibly by approximately 50% upon touching, which is readily measured using a capacitance meter. The response of the sensor does not degrade when cycled repeatedly at subzero temperatures. One can readily envision use of this sensor in applications under a broad range of environmental conditions, including stretchable and rollable keypads and pressure sensors for soft robotics.

In summary, we have developed a class of hydrogels that retain high stretchability, high fracture toughness, and good conductivity at temperatures far below the freezing point of water. We adopted a well-known strategy for depressing the freezing point of water and applied it to a tough hydrogel by soaking the gel in various aqueous solutions of $CaCl_2$. The experimental phase diagram of the $CaCl_2$-containing hydrogel differs from that of the aqueous $CaCl_2$ solution due to the presence of the polymer network and stresses the difference of $CaCl_2$ concentration inside the gel and in the soaking solution. Depending on the temperature and the $CaCl_2$ content, the gels can be classified into three types: regular hydrogel, slurry gel, and fully frozen gel. We measured the stress–stretch curves and fracture toughness of the hydrogel as a function of temperature and $CaCl_2$ content. Slurry gels exhibit the highest toughness at a given temperature. We attributed this observation to the introduction of additional toughening mechanisms in the slurry gels, which include crack pinning, crack deflection, and energy dissipation through micro-cavitation. Finally, we demonstrated a stretchable ionic touch sensor that functions at temperatures well below the freezing point of water. We anticipate that this class of hydrogels will enable a broad range of applications under low-temperature conditions.

Experimental Section

Hydrogel Synthesis: All chemicals were received and used without further purification. The following substances were purchased from Sigma-Aldrich: acrylamide (AAm, A8887), ammonium persulfate (APS, A9164), N,N,N′,N′-tetramethylenediamine (TEMED, T7024), N,N′-methylenebis(acrylamide) (MBAA, M7279), calcium sulfate dihydrate (CaSO₄·2H₂O, C3771), and calcium chloride ($CaCl_2$, C1016). Sodium alginate was purchased from FMC Biopolymer (Manugel GMB). Polyacrylamide-alginate double-network hydrogels were prepared following the method described by Sun et al.[3] First, 40.54 g of AAm and 6.76 g of sodium alginate powder were dissolved in 300 mL of distilled water to form an aqueous solution. The solution was stirred overnight for complete mixing. Afterward, MBAA, TEMED, APS, and CaSO₄·2H₂O in quantities of 0.0006, 0.0025, 0.01, and 0.022 times the weight of AAm were added to the solution in sequence. The prepared pregel solution was then degassed, quickly poured into $50 \times 40 \times 1.65$ mm³ acrylic molds, and covered with a glass plate. The samples were kept at room temperature for 24 h to allow complete polymerization. Afterward, the samples were taken out of the molds and were either directly used for testing (referred as 0 wt% $CaCl_2$ gels) or soaked in 10 or 30 wt% $CaCl_2$ solutions for at least 5 d. To ensure that the concentration of $CaCl_2$ in the external solution remained nearly constant before and after soaking the hydrogel, we prepared the $CaCl_2$ solution with a volume at least 10 times the volume of the hydrogel. The final water contents of the 0, 10, and 30 wt% $CaCl_2$ gels were 76%, 84%, and 78% by weight, respectively. It is worth noting that the precise control of the water content for the different gel compositions is difficult and was not the focus of the present study. Instead, a simple and easily reproducible method for preparing the different gel compositions was chosen. Extensive research on the effect of water content has been conducted and discussed in prior

work.[3,22] Eventually, considering the 0 wt% $CaCl_2$ gel as the reference state, the volumetric swelling ratios reached by the 10 and 30 wt% $CaCl_2$ gels were ≈1.78 and ≈2.20, respectively.

Mechanical Testing: A minimum of three specimens were used for all test conditions. The nominal stress–stretch curves were tested using the pure shear setup,[3,21] both at ambient and subzero temperatures (i.e., 20, 0, −15, −30, −50, and −70 °C); see Figure S3 (Supporting Information) for the full set of data. A thin sheet of hydrogel sample with a rectangular shape (50 mm width and 10 mm length) was fixed to two rigid acrylic grips, and mounted in an Instron 5966 tensile tester with a 500 N load cell. The temperature of the ambient environment was controlled by an Instron 3119-600 environmental chamber supplied with liquid nitrogen. Tensile tests were performed at a strain rate of 1 min⁻¹ and video-recorded with a digital camera (Canon 7D). The nominal stress was computed by dividing the applied load on the sample by its initial cross-sectional area (the product of width times thickness), while the stretch was calculated by dividing the deformed length by the initial length of the sample. To avoid undercooling of the hydrogel samples, specimens were first held at −90 °C for 45 min and then 20 min at the final testing temperature to ensure equilibrium conditions for each experiment (see Figure S5, Supporting Information).

To measure the fracture toughness, specimens were cut using a fresh razor blade to create a 20 mm notch extending from the edge of the specimen. The stress–stretch curves of identical specimens with and without notch were then measured. The critical stretch for fast fracture of the notched specimens was measured and the associated critical energy release rate was then determined using the method developed by Rivlin and Thomas[21]

$$G = W(\lambda_c)H \tag{1}$$

where H is the initial length of the sample and $W(\lambda)$ is the area below the nominal stress-stretch curve of the unnotched sample integrated up to the critical stretch λ_c of the notched sample.

Thermal Characterization: Samples were characterized using a differential scanning calorimeter (TA Instruments, DSC Q200) with a refrigerated cooling system (TA Instruments, RCS90). Samples were contained in hermetically sealed aluminum pans (TA Instruments, Tzero Aluminium Hermetic Pan) for testing, with an empty pan used as inert reference. The DSC was operated under a 40 µL min⁻¹ nitrogen flow rate and data were captured at a rate of 1 Hz. Samples were first equilibrated at 25 °C and then cooled at a rate of 5 °C min⁻¹ to −90 °C. After an isothermal period of at least 90 min, samples were heated up at 1 °C min⁻¹ to the initial equilibration temperature (25 °C).

Conductivity Measurement: The current passing through a rectangular gel specimen was measured as a function of the applied voltage (five measurements ranging from 0.1 to 1 V) with a two-point probe set up. Sample dimensions were measured to within 0.1 mm. The conductivity of the sample was deduced from the slope of current versus voltage. The measurement was performed for each gel composition at temperatures ranging from room temperature to −50 °C.

Ionic Touch Sensor Demonstration: A sensor that can detect the pressure of finger touch in a design similar to previous work was fabricated.[7] The sensor consisted of a $20 \times 20 \times 0.5$ mm³ acrylic elastomer (VHB 4905, 3M), covered with two 30 wt% $CaCl_2$ hydrogels of $20 \times 20 \times 0.2$ mm³ on each side. Copper wires were used to connect the hydrogels to metallic electrodes and the electrodes to a capacitance meter (LCR/ESR meter, Model 885, BK Precision). The capacitance meter was set to a sinusoidal measurement signal with a maximum voltage of 1 V and a frequency of 100 Hz. To demonstrate the sensing ability at low temperature, the sensor was attached to a glass plate, and the change of capacitance as a result of repeated touches at −11 °C was recorded.

Supporting Information

Supporting Information is available from the Wiley Online Library or from the author.

**ADVANCED
SCIENCE NEWS**
www.advancedsciencenews.com

**ADVANCED
MATERIALS**
www.advmat.de

[1] a) R. Langer, *Nature* **1998**, *392*, 5; b) K. Y. Lee, D. J. Mooney, *Chem. Rev.* **2001**, *101*, 1869; c) J. L. Drury, D. J. Mooney, *Biomaterials* **2003**, *24*, 4337.

[2] a) J. P. Gong, Y. Katsuyama, T. Kurokawa, Y. Osada, *Adv. Mater.* **2003**, *15*, 1155; b) K. J. Henderson, T. C. Zhou, K. J. Otim, K. R. Shull, *Macromolecules* **2010**, *43*, 6193; c) J. Li, W. R. Illeperuma, Z. Suo, J. J. Vlassak, *ACS Macro Lett.* **2014**, *3*, 520.

[3] J.-Y. Sun, X. Zhao, W. R. Illeperuma, O. Chaudhuri, K. H. Oh, D. J. Mooney, J. J. Vlassak, Z. Suo, *Nature* **2012**, *489*, 133.

[4] C. Keplinger, J. Y. Sun, C. C. Foo, P. Rothemund, G. M. Whitesides, Z. Suo, *Science* **2013**, *341*, 984.

[5] W. R. Illeperuma, P. Rothemund, Z. Suo, J. J. Vlassak, *ACS Appl. Mater. Interfaces* **2016**, *8*, 2071.

[6] a) C. Larson, B. Peele, S. Li, S. Robinson, M. Totaro, L. Beccai, B. Mazzolai, R. Shepherd, *Science* **2016**, *351*, 1071; b) C. H. Yang, B. Chen, J. Zhou, Y. M. Chen, Z. Suo, *Adv. Mater.* **2016**, *28*, 4480.

[7] J. Y. Sun, C. Keplinger, G. M. Whitesides, Z. Suo, *Adv. Mater.* **2014**, *26*, 7608.

[8] C.-C. Kim, H.-H. Lee, K. H. Oh, J.-Y. Sun, *Science* **2016**, *353*, 682.

[9] M. Wehner, R. L. Truby, D. J. Fitzgerald, B. Mosadegh, G. M. Whitesides, J. Lewis, R. J. Wood, *Nature* **2016**, *536*, 451.

[10] H. Gao, Z. Zhao, Y. Cai, J. Zhou, W. Hua, L. Chen, L. Wang, J. Zhang, D. Han, M. Liu, *Nat. Commun.* **2017**, *8*, 15911.

[11] a) G. Wieslander, D. Norbäck, T. Lindgren, *Occup. Environ. Med.* **2001**, *58*, 649; b) D. A. Pillard, *Environ. Toxicol. Chem.* **1995**, *14*, 311; c) J. R. Fowles, M. I. Banton, L. H. Pottenger, *Crit. Rev. Toxicol.* **2013**, *43*, 363; d) A. Mohiley, J. Franzaring, O. Calvo, A. Fangmeier, *Environ. Sci. Pollut. Res.* **2015**, *22*, 13094.

[12] W. Illeperuma, Z. Suo, J. J. Vlassak, *Google Patents* *WO2017040851A1*, **2017**.

[13] M. R. Conde, *Int. J. Therm. Sci.* **2004**, *43*, 367.

[14] a) W. H. Rodebush, *J. Am. Chem. Soc.* **1918**, *40*, 1204; b) S. A. Ketcham, L. D. Minsk, R. R. Blackburn, E. J. Fleege, *Manual of Practice for an Effective Anti-icing Program: A Guide for Highway Winter Maintenance Personnel*, FHWA-RD-95-202, Federal Highway Administration, **1996**; c) *Calcium Chloride Product Datasheet*, http://www.oxy.com/OurBusinesses/Chemicals/Products/Documents/CalciumChloride/173-01791.pdf (accessed: March 2018).

[15] *Techniques for Winter Road Maintenance*, http://epdfiles.engr.wisc.edu/pdf_web_files/tic/bulletins/Bltn_022_prewetting_antiicing.pdf (accessed: March 2018).

[16] a) W. Block, *Funct. Ecol.* **1991**, *5*, 284; b) J. G. Duman, D. W. Wu, L. Xu, D. Tursman, T. M. Olsen, *Q. Rev. Biol.* **1991**, *66*, 387; c) I. K. Voets, *Soft Matter* **2017**, *13*, 4808.

[17] Y. Bai, B. Chen, F. Xiang, J. Zhou, H. Wang, Z. Suo, *Appl. Phys. Lett.* **2014**, *105*, 151903.

[18] a) A. Kinloch, S. Shaw, D. Tod, D. Hunston, *Polymer* **1983**, *24*, 1341; b) R. A. Pearson, A. F. Yee, *J. Mater. Sci.* **1986**, *21*, 2475; c) H. E. Meijer, L. E. Govaert, *Prog. Polym. Sci.* **2005**, *30*, 915; d) A. Kinloch, R. Mohammed, A. Taylor, C. Eger, S. Sprenger, D. Egan, *J. Mater. Sci.* **2005**, *40*, 5083.

[19] a) A. J. Crosby, K. R. Shull, H. Lakrout, C. Creton, *J. Appl. Phys.* **2000**, *88*, 2956; b) H. Lakrout, P. Sergot, C. Creton, *J. Adhes.* **1999**, *69*, 307.

[20] K. Brown, C. Creton, *Eur. Phys. J. E: Soft Matter Biol. Phys.* **2002**, *9*, 35.

[21] R. Rivlin, A. G. Thomas, *J. Polym. Sci., Part A: Polym. Chem.* **1953**, *10*, 291.

[22] a) E. Zhang, R. Bai, X. P. Morelle, Z. Suo, *Soft Matter* **2018**, *14*, 3563; b) J. Li, Y. Hu, J. J. Vlassak, Z. Suo, *Soft Matter* **2012**, *8*, 8121; c) W. Hong, Z. Liu, Z. Suo, *Int. J. Solids Struct.* **2009**, *46*, 3282.

1801541 (8 of 8)